RSC Advances

ROYAL SOCIETY OF CHEMISTRY

www.rsc.org/advances

Effect of additives on the properties of electrodeposited Ni-zircon composite coatings

S.T. Aruna*, P.G. Lashmi, H.M. Seema
Surface Engineering Division,
Council of Scientific and Industrial Research-National Aerospace Laboratories,
HAL Airport Road, Bangalore 560017, India

Abstract:

In the present study, the suitability of zircon powder as a new distributive phase for electrodeposited Ni composite coating is explored. Ni-zircon composite coatings are electrodeposited from a nickel sulfamate bath. Ball-milled zircon mineral powder with an average particle size of 0.13 μm has been used as the new distributive phase. The optimized particle loading and current density are 50 g/L and 0.77 Adm^{-2} respectively. The influence of additives like coumarin and cetyl trimethylammonium bromide (CTAB) on the properties of electrodeposited Ni-zircon coatings is reported. Ni-zircon coating containing coumarin exhibits highest microhardness (~650 HK at 50gF load) and poor corrosion resistance. The poor corrosion resistance is attributed to the presence of cracks. Experimental results show that CTAB addition is very effective in increasing the amount of zircon particles in the Ni matrix. CTAB acts as an effective surfactant and decreases the agglomeration of particles in the Ni matrix. This results in a more uniform distribution of zircon particles in the nickel matrix. A synergistic combination of higher microhardness and corrosion resistance is imparted to Ni-zircon composite coating by the addition of CTAB to the nickel sulfamate bath.

Keywords: Electrodeposition; Ni; Particles; Additives; Microhardness; Corrosion

* Corresponding author
Tel.: +9180 25086250
Fax: (080) 2521-0113
E-mail address: aruna_reddy@nal.res.in

1. Introduction

Electrodeposition is a fascinating and handy technique that is widely used to perceive the properties of composite coatings in which second phase particles are dispersed in metal matrix [1]. Compared to the plain metallic coatings, composite coatings exhibit improved physical and electrochemical properties. Among the electrodeposited composite coatings, Ni coatings containing inert particles are widely reported. In nickel composite coatings, during co-electrodeposition, solid insoluble materials are suspended in a conventional plating electrolyte and captured in the growing metal film. For nickel matrix electrodeposits in particular, a variety of particles such as hard oxides (Al_2O_3, TiO_2, SiO_2), carbides (SiC, WC), diamond, solid lubricants (PTFE, graphene, MoS_2), carbon nanotubes, diamond, pumice etc have been used [2-10]. The properties of metal matrix composites depend on the type and amount of particles incorporated within the matrix. The deposited particle concentration in the nickel matrix mainly depends on parameters like bath composition, deposition variables and particle properties. The particle properties include the material, size, shape and particle size distribution. Electrodeposited Ni-SiC is the most widely studied and commercially used coating [11]. However, the interfacial reaction between nickel and SiC has limited the application of nickel composite coatings containing SiC particles in high temperature environment, such as diesel engine cylinder (above 500°C) and automobile engine exhaust pipe (about 600 °C) [12]. Therefore oxide particles are being investigated as distributive phase in Ni composite coatings more critically to overcome this problem. So researchers are exploring new distributive phases for incorporation in Ni-matrix. Among the naturally available minerals zircon seems to be an interesting material. Zircon is produced as one of the several products from heavy-mineral sand deposits associated with ancient shorelines. Zircon has been recognized as a potential structural material because of its good combination of physical and mechanical properties, such as excellent chemical stability, thermal shock resistance, strength retention to high temperatures and low thermal expansion as well as low heat conductivity [13]. The chemical name of zircon is zirconium silicate ($ZrSiO_4$). It is chemically inert and stable up to very high temperatures. The crystal structure of zircon is tetragonal and its natural color of zircon varies between colorless to red brown to yellow-golden and green [14].

In the conventional methods of electrodeposition, one problem is that when the particle size is small, particularly in nano and submicron, particle agglomeration occurs easily due to high surface activity of the nanoparticles. There are reports on the addition of metal cationic accelerants and organic surfactants in the electrolytic bath to prevent agglomeration and improve the amount and distribution of co-deposited particles [15]. Coumarin is used as an additive in nickel electroplating baths, especially semi-bright nickel processes, to produce ductile, lustrous deposits with excellent levelling [16]. The surfactant CTAB (cetyltrimethyl ammonium bromide), a cationic surfactant is considered as having good potential in the application of nano-technology because it strongly adsorbs on nano particles [17]. Besides, CTAB is also used as a corrosion inhibitor. There are studies on the effect of CTAB surfactant and stirring speed on the particle size distribution, microhardness and wear resistant properties of electrodeposited Ni-SiC metal matrix composite coating on steel surfaces [18-20]. From the literature survey it is evident that there are no studies on Ni-zircon composite coatings and the effect of additives on the properties of Ni composite coating.

The main objectives of the present work are: (i) To codeposit zircon powder with Ni matrix to prepare Ni-zircon electrocomposite coating, (ii) To study the effect of additives like coumarin and CTAB on the properties of electrodeposited Ni-zircon coating.

2. Experimental

2.1. Powder processing and its characterization

Yellow colored zircon powder (CUMIcoat ZR101) was received from M/s. Carborundum Universal Ltd. Since the particles were coarser with an average agglomerated particle size of 11.65 μm, the powder was subjected to ball milling using Fritsch Pulverisette unit at 250 rpm for 4 h using zirconia balls as the grinding media and ethanol as the solvent. The milled fine powder was dried in an oven at 100 °C and then used for electrodeposition. The crystalline phases present in the ball milled zircon powder was confirmed by powder X-ray diffractometry. The particle size distribution of the ball milled zircon powder was determined using particle size analyser based on laser diffraction (Malvern, Mastersizer 2000). The morphology of the ball-milled zirconia powder was studied by using a field emission scanning electron microscope (Carl Zeiss Supra 40).

2.2. Electrodeposition of Ni-zircon composite coatings

About 200 mL of the nickel-sulfamate solution was taken in a beaker and sodium lauryl sulfate (0.2 g/L) was added to it and the pH of the bath was maintained at 4.0. More details regarding the nickel sulfamate bath preparation and composition is provided in Table-1. A brass substrate was made as cathode and a nickel rod of same dimension was used as anode. For composite coating development, ball-milled zircon powder (25, 50 and 100 g/L) was dispersed in a nickel sulfamate bath and kept for overnight stirring. Then electrodeposition was carried out using an Aplab 7253 regulated DC power supply at different current densities: 0.77 A dm^{-2} for 6 h, 1.55 A dm^{-2} for 3 h, 3.1 A dm^{-2} for 1.5 h and 5.4 A dm^{-2} for 45 min such that the deposit thickness was ~ 40 μm based on Faraday's laws. To study the effect of additives like coumarin and CTAB, 0.18 g/L of the additives were added to the above said nickel sulfamate bath containing 50 g/L of zircon. The concentration of additives was fixed based on the literature report [21]. The optimized plating conditions of 50 g/L and 0.77 Adm^{-2} were used for the electrodepositions in presence of additives. Sodium lauryl sulphate (2 g/L) was also added to the nickel sulfamate bath containing powder and stirred well to avoid the pits formation. The obtained Ni-zircon, Ni-zircon-coumarin and Ni-zircon-CTAB coatings are hereinafter designated as Ni-Zr, Ni-Zr-CM and Ni-Zr-CT respectively.

2.3. Characterization of electrodeposited Ni-zircon composite coating

The powder XRD patterns of plain Ni and Ni-zircon composite coatings electrodeposited at 0.77 A dm^{-2} were also recorded and the relative texture coefficients $RTC_{(hkl)}$ were also calculated. The texture and preferred orientation of the nickel films was estimated using the relative texture coefficient RTC_{hkl} using equation 1 [22]:

$$RTC_{hkl} = \frac{I_{hkl} / I^{0}_{hkl}}{\sum_{1}^{3} I_{hkl} / I^{o}_{hkl}} .100\% \quad \ldots\ldots\ldots\ldots\ldots\ldots\ldots\ldots (1)$$

where I_{hkl} are the relative intensities of the (hkl) reflections, Σ I_{hkl} is the sum of all intensities, in our case (111), (200), and (220). The superscript ° refers to the relative intensities of a randomly oriented nickel powder sample (JCPDS no. 4-850). The preferred

orientation through an axis [hkl] is selected by values of RTC≥16.67% such that when the RTC approaches the value of 100%, the strength of the preferred orientation becomes maximum amount [22].

Energy dispersive X-ray Spectroscopy (EDS, Oxford instrument's Inca Penta FET X3 model) integrated with FESEM instrument was used for elemental analysis of the electrodeposited Ni composite coatings. The microhardness of the coatings was investigated using microhardness tester (Micromet 2103) with a load of 50 gF and a Knoop indenter was used for the measurement. The optical micrographs of the electrodeposited coatings were recorded using a vertical metallurgical microscope (Leica DM-1RM). For cross-sectional microscopic analysis, metallographic specimens were prepared by sandwiching the electrodeposited coating with a copper backup in a Bakelite matrix. This was followed by mechanical grinding using emery sheets of different grades (100, 180, 240, 400, 600, 800, 1000 and1200 μm) and polishing with Al_2O_3 slurry, down to 0.05 μm.

Using CHI 604 2D electrochemical workstation the corrosion behavior of Ni and Ni-Zr coatings on mild steel coupons with an active area of $1cm^2$ were studied using a flat cell. The corrosion test was carried out with non-deaerated 3.5 wt% (0.6 M) NaCl solution (200 ±2 mL) using conventional three electrode cell. The electrodeposited coatings acted as working electrode. A platinum foil was used as the counter electrode and the saturated calomel electrode (SCE) was used as the reference electrode. In order to minimize the IR drop, the reference electrode was connected to a Luggin capillary and its tip was placed very close to the surface of the working electrode. The coated coupon was immersed in NaCl solution for 50 min to establish the open circuit potential (E_{OCP}). The EIS was studied in the frequency ranging from 100 kHz - 10 mHz. The amplitude of applying the alternating potential was on the E_{OCP} with 10 mV. The impedance data were displayed in the form of Nyquist plot of real (Z′) vs. imaginary impedance (Z″). After the EIS measurements, the system was allowed to attain the open circuit potential and then the upper and lower potential limits of linear sweep voltammetry were set at ±200 mV with respect to the E_{OCP} and the sweep rate was 1 mV/s. The acquired data were curve fitted and analyzed using ZSimpwin program. The Tafel plots are representation of potential vs. log i plot.

3. Results and Discussion

The ball-milled zircon powder showed an average agglomerated particle size of 0.13 μm. Fig.1. shows the powder XRD pattern of zircon powder. The powder is highly crystalline as evident from the sharp peaks. Most of the XRD peaks matched the tetragonal zircon phase (JCPDS card no. 06-0266).The peak observed at $2\theta = 24.3^\circ$ may be assigned to the monoclinic (110) peak (JCPDS card no.17-923) of zirconia. Fig. 2 shows the FESEM image of ball milled zircon powder. The particles were blocky angular in shape and their size varied, some smaller sized spherical particles were also observed.

The mechanism of codeposition of zircon particles in the nickel matrix may be speculated as follows: Nickel ionic clouds are formed around the zircon particles in the bulk electrolyte, followed by the convective movement of the particle along with the ionic cloud towards the cathode; the ionic cloud diffuses through a concentration boundary layer and electrical double layer (typical dimensions of nm) followed by adsorption on the cathode and entrapment of particles along with the reduced nickel ions [23].

Fig.3. shows the variation of microhardness with different current densities used for the electrodeposition of Ni-zircon coatings from Ni sulfamate bath with particle loadings of 10, 50 and 100 g/L. Irrespective of the particle loading, higher microhardness was observed for coatings obtained at lower current density. From figure 3, it is evident that for the Ni-Zircon composite coatings electrodeposited from 50 g zircon /L bath, the Knoop microhardness was higher at all current densities. Interestingly, the higher concentration of particles did not facilitate higher incorporation of the particles. So, for further studies, composite coatings were electrodeposited in presence of coumarin and CTAB from 50 g/L zircon particles loaded bath at the lowest current density of 0.77 A/dm^2.

The microhardness was found to be 280 KHN for plain Ni electrodeposited at 0.77 A/dm^2 at an applied load of 50 gF. The composite coatings displayed higher microhardness compared to plain Ni coating. The increased microhardness of Ni-Zr composite coatings compared with nickel coating without any reinforced particles might be due to the influence of hard nature of the zircon particles (hardness of 7.5 Mohs) and the strengthening effect with the incorporation of inert particles. The variation of microhardness of Ni-Zircon coatings with various concentrations of particles is shown in Fig. 3. From the histogram it is observed that irrespective of the bath loading, the lowest current density (0.77 A/dm^2) increased with increasing particle loading in the bath and it did not change much with higher particle loading as it reaches a saturation point. The reasons for increased microhardness of nickel composite

coatings with the incorporation of particles may be attributed to the fact that the particles act as small barriers, which inhibit easy dislocation movements and increase the coating hardness (according to Orowan mechanism) [24]. Fig.4 shows the Knoop microhardness values of Ni-zircon coatings electrodeposited at 0.77 A/dm^2 from 50 g/L bath with and without additives. It was found that maximum microhardness of 648 KHN was observed for Ni-zircon composite coating containing coumarin despite lower % of particle incorporation. In fact, the hardness of composite coatings is influenced by two aspects: one is the amount of incorporated hard particles, which increase the hardness of composite coatings; the other is the hardness of metal matrix, which is determined by the electroplating parameters. Coumarin being a levelling agent (brightener) is effective in increasing the hardness of electrodeposited nickel due to the incorporation of melilotic acid formed by the cathodic reduction of coumarin and in turn lowering its ductility and raising its hardness, but tend to raise internal stress [25]. The cross-sectional optical micrographs of Ni-Zircon composite coatings obtained at 0.77 A/dm^2 with 50g/L particle loadings in the bath are shown in Figure 5. From the optical images of Ni-Zr-CT composite coating it is evident that in presence of CTAB, more zircon particles are incorporated in the nickel matrix and also the particles are free from agglomeration. This may be attributed to the modification of the surface charge of the zircon particles by the absorbed CTAB which is a key factor for preventing of the agglomeration [26]. All the electrodeposited Ni-Zr coatings possessed good adhesion to the substrate as evident from the cross-sectional optical microscope images. The area fraction of particles incorporated in Ni-zircon coating was highest with CTAB (17%) followed by coating without any surfactant (10%) and was least for the coating with coumarin (8%). This has been reflected in the higher current efficiency of this coating (182%) and higher coating thickness compared to other coatings. The enhancement in area fraction of particles is considered to be associated with the modification of the surface charge of the particles by the absorbed molecules or ions, thereby promoting electrophoretic migration of the suspended particles. It can be concluded that adsorption of a cationic surfactant like CTAB develops a positive charge on the particle surface which prevents the particle from being agglomerated, and hence, increases the stability of the particle suspension in the bath. On the other hand, the developed positive surface charge increases the affinity of these particles towards cathode and increases the particle co-deposition into a metal matrix. [15].

Fig.6. shows the XRD patterns of Ni-Zr composite coatings. All the patterns showed Ni(111) as the major peak. Only in the XRD pattern of Ni-Zr-CT, peak due to zircon was visible which was also reflected in the higher area fraction of particles.

The diffractograms of Ni and Ni-Zr composite coatings is characterized by mainly three diffraction peaks (111), (200) and (220), which corresponds to [111], [100] and [110] preferred orientation. A reflection at 2θ=27° corresponding to (200) plane of zircon was observed in Ni-Zr-CT and it is not clearly observed due to the relatively high intensity of nickel diffraction peaks. A change in relative intensity of the nickel diffraction peaks occurred with the incorporation of zircon particles and additives. Coumarin addition did not alter the intensity to a greater extent. However, CTAB addition altered the intensity of (200) peak and an additional Ni peak corresponding to Ni(110) was observed. These changes can be expressed through the value of the relative texture coefficient of each crystalline orientation. Embedding of zircon particles in the nickel matrix provokes changes in the structure of pure nickel coatings. According to literature data the codeposition of oxides with nickel results in textural modifications compared to those observed for pure nickel deposits and is correlated to the particle loading in the bath and surface properties of the dispersoids. With zircon loading, the region of deposits oriented through [111] axis is reduced and replaced by composites exhibiting mixed [111] and [100] texture [27]. This may be attributed to the changes taking place in the nature of adsorption desorption phenomena in the region of the catholyte area when surface charged oxides arrive at the cathode and are loosely adsorbed or partially submerged onto the growing nickel grains. Thus the observed textural modifications of composite coatings are associated with specific structural modifications of Ni crystallites provoked by the adsorption–desorption phenomena occurring on the metal surface, induced by the presence of particles. There was a drastic reduction in the $RTC_{(111)}$ value corresponding to Ni-Zr-CT compared to Ni, Ni-Zr and Ni-Zr-CM, the RTC reduced from 22.96 to 11.16. Interestingly, the $RTC_{(200)}$ increased from 17.93 to 39.36 with the incorporation of zircon particles. This may be attributed to the different surface morphologies observed for the electrodeposited composite coatings.

The FESEM images of Ni-Zr coating obtained at 0.77 A/dm^2 (50 g/L) are shown in Fig. 7. The Ni-Zr composite coating exhibited some irregular nodular features. Ni-Zr-CM coating consisted of fine grained crystals and is attributed to the presence of coumarin as it is well known as an excellent leveling agent that produces fine-grained deposits and flat crystals.

The nodular features are reduced in coatings prepared from baths containing coumarin and CTAB. The grain refinement is caused by the combined effect of additives: (i) increasing nucleation frequency caused by blockage of crystal growth, (ii) retaining diffusion of nickel adatoms on the cathode surface and (iii) lowering of the over potential for the reduction of Ni^{+2} ions. [27]. Although the nodular features decreased with the addition of coumarin, a higher magnification FESEM image of the Ni-Zr-CM coating showed the presence of cracks. This may be due to the incorporation of melilotic acid formed by the cathodic reduction of coumarin. From higher magnification FESEM images of the coatings surface, it is observed that Ni-Zr-CT composite coating consists of spherical globules. The composition of the Ni-zircon composite coating was verified by EDS spectrum which exhibited peaks corresponding to O, Si, Ni, and Zr (Table-2). Higher wt% of Zr and Si was observed with Ni-Zr-CT coating.

The plots of open circuit potential vs. time for Ni, Ni-Zr, Ni-Zr-CM and Ni-Zr-CT coatings are shown in Fig.8. From the plot it is evident that the potential is stabilized in all the coatings within 50 min. The potentiodynamic polarization curves for Ni, Ni-Zr composite coatings with and without surfactants are shown in figure 9. The corrosion potential, corrosion current and the polarization resistances are represented in Table-3. On comparing the corrosion potentials of Ni-Zr, Ni-Zr-CT composite coatings with Ni, it is evident that there is a greater shift of potential towards more positive side for these coatings which clearly depicts the improved corrosion resistance of the coatings; while that of Ni-Zr-CM shifted towards negative side indicating relatively lower corrosion resistance. In addition to this, the kinetics of corrosion reaction can be evaluated by corrosion current density as the corrosion protection and current density are inversely proportional. The corrosion current density for Ni-Zr-CT coatings was very low with very high R_p value indicating improved corrosion resistance compared to other coatings (Table-3).

The Nyquist plots of Ni and Ni-Zr composite coatings are shown in Figure 10. In the Nyquist plot, each point is recorded at particular frequency such that the low frequency data are on the right side of the plot and the high frequency data are on the left. So the interception with the real axis at high frequencies is attributed to the electrolyte bulk resistance (R_s) and the low frequencies to the charge transfer resistance (R_{ct}).The shape of the impedance spectra describes the type of the chemical reaction taking place on the surface of the electrodes. From the Nyquist plot it is obvious that the impedance offered by Ni-Zr-CT is higher than Ni-Zr, Ni-Zr-CM and plain Ni coatings. In the Nyquist plot, the diameter of the semicircle

corresponding to Ni-Zr-CT coating is highest compared to other coatings, indicating better corrosion resistance of the coating. The electrochemical impedance data reveals that Ni-Zr-CT coating has highest R_{ct} value which accounts for higher corrosion resistance. The impedance plot of Ni, Ni-Zr, Ni-Zr-CT shows single time constant and Ni-Zr-CM shows two time constant behaviour (Fig.10 inset). The higher-frequency component is related to the electrolyte/coating interface and the lower frequency component to the substrate/electrolyte interface.

Bode Plots of Ni and Ni-Zircon composite coatings are shown in Figure 11. For all the coatings, the phase angle was less than 90^o. The fitted values of electrochemical impedance data is displayed in Table 4. The fitted curves are also shown in the respective impedance plots. In all cases, good conformity between theoretical and experimental data was ensured for the whole frequency range and quality of the fit was checked by the χ^2 value. The non-ideal capacitive response of the coatings was entailed by using a constant phase element (CPE) instead of a pure capacitance in the fitting procedure. This CPE can be due to difference in the relaxation times as a result of different degrees of surface in-homogeneity, roughness factors and compositions of surface layers.

The polarization resistance values (R_p) obtained by polarization studies for Ni and other composite coatings are comparable to R_{ct} values from EIS. The charge transfer resistance of Ni–Zr-CT coating is the highest (258 $k\Omega cm^2$), which indicates that resistance offered by the coating is higher. The ndl values for all the nanocomposite coatings are in the range of 0.88 to 0.93 indicating a deviation in the behavior of surface of the coatings from ideal capacitive behavior.

A lower C_{dl} value was observed for Ni-Zr-CM coating which may be attributed to the presence of micro cracks on the coating surface. The equivalent circuits of plain Ni and Ni-Zr composite coatings are given in Figure 12. Plain Ni, Ni-Zr and Ni-Zr-CT composite coatings were fitted with single time constant; Ni-Zr-CM composite coating was fitted with two time constants. This indicates that the surface of Ni-Zr-CM coating was extensively exposed to corrosive media due to the presence of cracks on the surface of the coating. From the potentiodynamic and impedance studies, it can be concluded that the corrosion resistance properties of the coatings decreased in the following order: Ni-Zr-CT>Ni-Zr>Plain Ni >Ni-Zr-CM.

4. Conclusions

The main objective of this study was to investigate the suitability of zircon powder as a new distributive phase for electrodeposited Ni composite coating. The study was also aimed at investigating the effect of additives like coumarin and CTAB on the properties of electrodeposited Ni-zircon composite coating. The highlights of the study are as follows:

- Zircon is a naturally available mineral which is cheaper compared to the oxides and SiC powders that are employed in the composites development.
- Coarse zircon mineral powder was ball-milled to get fine powder with an average agglomerated particle size of 0.13 μm. The ball milled powder was successfully incorporated into the Ni matrix by electrodeposition using a nickel sulfamate bath
- The effect of particle loading and current density was studied on the microhardness of the Ni-zircon coating and the optimized condition was found to be 0.77 Adm^{-2} with a particle loading of 50 g/L
- Ni-Zr coating showed higher microhardness compared to plain Ni coating
- Ni-zircon composite coatings with additives like coumarin and CTAB were electrodeposited at the optimized parameters of 0.77 Adm^{-2} with a particle loading of 50 g/L
- The Ni-zircon coating containing coumarin exhibited highest microhardness but the coating showed cracks due to internal stress
- Large fraction of zircon particles were incorporated in the electrodeposited Ni-Zr-matrix in the presence of CTAB. CTAB also inhibited the agglomeration of particles.
- The extent of nodularity of electrodeposited Ni-Zr composite coatings decreased in the presence of coumarin and CTAB
- Ni-Zr-CT coating exhibited improved corrosion resistance compared to other coatings.

The present study proves beyond doubt that zircon is a promising new distributive phase for electrodeposited Ni composite coatings and CTAB is a better additive compared to coumarin.

Acknowledgment

The authors are grateful to Director, CSIR-NAL and Head of surface engineering Division for their encouragement and support. The authors are also grateful to Mr. Siju, Dr. RPS Chakradhar, Mr. N.Balaji and S. Latha for their help in FESEM, XRD, particle size analysis, optical microscopy and microhardness analysis.

References

[1] H.Y. Ahmad and M. A. Adel Mohamed, *Int. J. Electrochem. Sci*, 2014, **9**, 1942.

[2] N. A. Badarulzaman, , S. Purwadaria, A. A. Mohamad and Z. A. Ahmad, *Ionics*, 2008, **15,** 603.

[3] S. Sadreddini and A. Afshar, *Appl. Surf. Sci***,** 2014, **303,** 125.

[4] M.R. Vaezi, S.K. Sadrnezhaad and L. Nikzad, *Colloids Surf A Physicochem Eng Asp***,** 2008, **315,** 176.

[5] M Surender, B Basu, R Balasubramaniam, *Tribol Int,* 2004, **37,** 743.

[6] W. Huang, Y.i Zhao and X. Wang, *Surf. Coat Technol,* 2013, **235**, 489.

[7] Y.-H.You, C.-D.Gu, X.-L. Wang, and J-P. Tu, *Int. J. Electrochem. Sci.,* 2012, **7,** 12440.

[8] C.M. Praveen Kumar,T.V. Venkatesha, and Rajashekhara Shabadi, *Mater. Res. Bull.,* 2013, **48**, 1477.

[9] S.T. Aruna, Shibayan Roy, A. Sharma, G. Savitha and V.K.William Grips, *Surf. Coat. Technol.,* 2014, **251**, 201.

[10] M.F. Cardinal, P.A. Castro, J. Baxi, H. Liang, F.J. Williams *Surf. Coat. Technol.,* 2009, **204**, 85.

[11] M.R. Vaezi, S.K. Sadrnezhaad and L. Nikzad, *Colloids Surf A Physicochem Eng Asp*, 2008, **315**, 176.

[12] A. Bachli, M.-A. Nicolet, L. Baud, C. Jaussaud, and R. Madar, *Mater. Sci. Eng., B,* 1998, **56,** 11.

[13] C. Aksel, Mater. Lett., 2002, **57**, 992.

[14] https://en.wikipedia.org/wiki/Zircon

[15] L.Chen, L. Wang, Z. Zeng and J. Zhang, *Mater. Sci. Eng.,A,* 2006, **A 434**, 319.

[16] S. Mohan, S. Shriram, S. Karthikeyan, Electrodeposition of nanocrystalline nickel, *Bull. Electrochem.* 2002, **18**, 241.

[17] Y. C. Chen, S.L. Kuo, J. L. Lee, S. T. Ke, C. H. Wong and M.D. Ger, *Key Eng. Mater.* 2008, **364-366**, 346.

[18] F. Kılıc¸ H. Gül , S. Aslan, A. Alp and H. Akbulut , *Colloids Surf A Physicochem Eng Asp* 419 (2013) 53.

[19] A. Fahami, B. Nasiri-Tabrizi, M. Rostami, and R. Ebrahimi-Kahrizsangi, ISRN Electrochem., 2013, Article ID 486050, 8 pages http://dx.doi.org/10.1155/2013/486050

[20] H. Gul, M. Uysal, H. Akbulut and A. Alp, *J. Composite Mater.,* 2015, 0021998315609974

[21] V. Kumar Bulasara, Ch. S. N. Mahesh Babu, R. Uppaluri, *Surf. Eng.*, 2012, **28**, 44.

[22] E.A. Pavlatou, M. Raptakis, N. Spyrellis, *Surf. Coat. Technol.,* 2007, **201**, 4571.

[23] C. T. J. Low, R.G.A. Walsh, F.C. Walsh, *Surf. Coat. Technol.,*2006, 201, 371.

[24] G. E. Dieter, Mechanical Metallurgy, third Edition, McGraw-Hill, New York, 1986.

[25] A. J. Dill, *Plating Surf. Finish.,* 1975, 62, 770.

[26] H. Gül, F. Kiliç, S. Aslan, A. Alp, and H. Akbulut, *Wear,* 2009, 267, **5-8**, 976.

[27] D.-H. Nam, K.-S Hong, J.-S Kim, J.-K. Lee, G.-E Kim and H.-S Kwon, *Surf. Coat. Technol.,* 2014, **248**, 30.

Figure captions

Fig.1. Powder X-ray diffractogram of zircon powders

Fig.2. FESEM image of ball milled zircon powder

Fig.3. Plots of variation of microhardness as a function of applied current density for 10, 50 and 100 g/L particle loading

Fig.4. Histogram showing the microhardness of Ni-Zr coatings with and without additives

Fig.5.Cross-sectional optical microscopy images of electrodeposited (a) N-Zr, (b) Ni-Zr-CM and (c) Ni-Zr-CT coatings

Fig.6. XRD patterns of (a) Ni, (b) Ni-Zr, (c) Ni-Zr-CM and (d) Ni-Zr-CT coatings

Fig.7. FESEM images of surface of (a),(b) N-Zr; (c),(d) Ni-Zr-CM; and (e), (f) Ni-Zr-CT coatings at two different magnifications respectively.

Fig.8. Plot of open circuit potential vs time for plain Ni, Ni-Zr, Ni-Zr-CM and Ni-Zr-CT composite coatings.

Fig.9. Tafel Plots of electrodeposited (a) Plain Ni (b) Ni-Zr, (c) Ni-Zr-CM and (d) Ni-Zr-CT composite coatings.

Fig.10. Nyquist plots of electrodeposited (a) Plain Ni (b) Ni-Zr, (c) Ni-Zr-CM and (d) Ni-Zr-CT composite coatings.

Fig.11. Bode Plots of electrodeposited (a) Plain Ni (b) Ni-Zircon composite coating (c) Ni-Zircon composite coating with Coumarin as surfactant (d) Ni-Zircon composite coating with CTAB as surfactant

Fig.12. Equivalent circuit (a) for plain Ni, Ni-Zr and Ni-Zr-CT composite coatings and (b) for Ni-Zr-CM composite coating (R_s is the solution resistance of electrolyte between working

electrode and the reference electrode; Q_{dl} double layer capacitance; Q_{coat} coating capacitance; R_{coat} coating resistance; R_{ct}charge transfer resistance; *WE* working electrode).

Tables

Table-1. Wt% of elements present in the Ni-Zr coatings as obtained from EDS analysis

Coatings	Composition (weight %)			
	Ni	Si	Zr	O
Ni-Zr	97.84±2.02	0.23±0.051	0.11±0.02	1.82±0.08
Ni-Zr-CM	98.30±1.98	0.18±0.045	0.10±0.18	1.42±0.07
Ni-Zr-CT	94.71±1.86	0.79±0.052	1.51±0.02	2.99±0.08

Table-2. Texture coefficients of Ni and Ni-Zr composite coatings

SAMPLE	Relative Texture Coefficient (%)	
	(111)	(200)
Plain Ni	22.96	17.93
Ni-Zr	21.09	39.36
Ni-Zr-CM	21.16	39.09
Ni-Zr-CT	11.16	30.23

Table-3. Potentiodynamic polarization data of electrodeposited Ni and Ni-Zr coatings

SAMPLE	I_{corr} ($\mu A\ cm^{-2}$)	E_{corr} (V)	R_p ($k\Omega cm^2$)
Ni	1.80	-0.314	25.10
Ni-Zr	0.58	-0.264	56.07
Ni-Zr-CM	3.39	-0.384	12.01
Ni-Zr-CT	0.14	-0.231	236.51

Table-4. Electrochemical impedance analysis data for Ni and Ni-Zr composite coatings

SAMPLE	R_s (Ωcm^2)	Q_{coat}-Y_0 ($\mu S\ s^n\ cm^{-1}$)	n_{coat}	R_{coat} (Ωcm^2)	Q_{dl}-Y_0 ($\mu S\ s^n\ cm^{-1}$)	n_{dl}	R_{ct} ($k\Omega cm^2$)
Ni	15	_	_	_	30.17	0.931	20.42
Ni-Zr	15.45	_	_	_	50.43	0.914	39.40
Ni-Zr-CM	10	61.81	0.587	5.54	40.92	0.928	14.12
Ni-Zr-CT	16.15	_	_	_	25.11	0.887	258.10

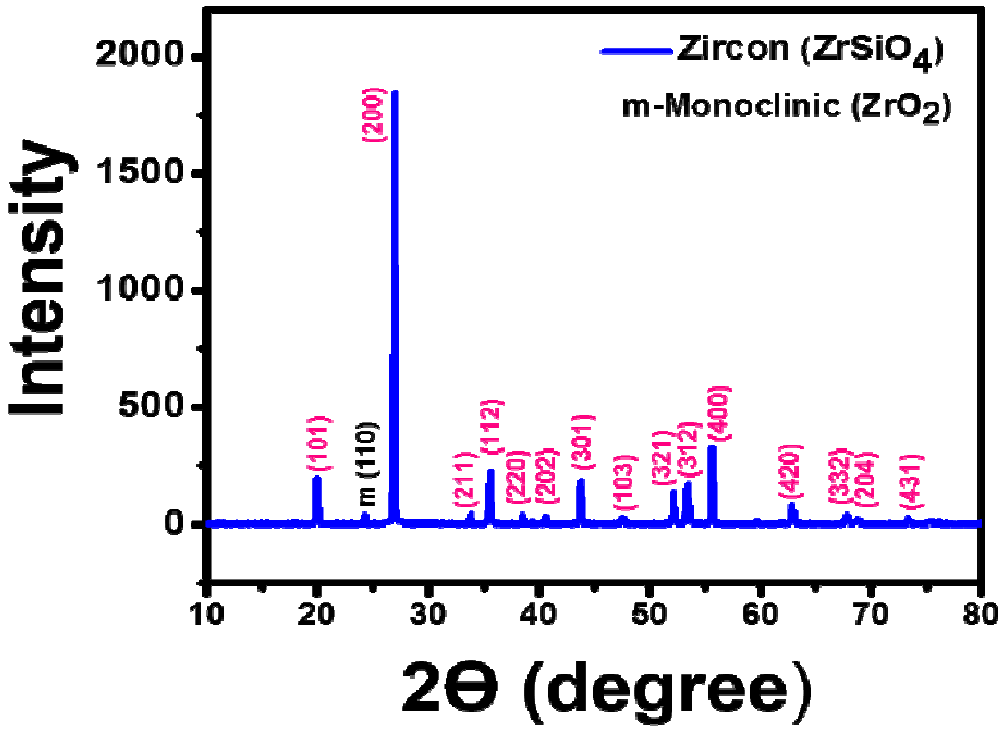

Fig.1

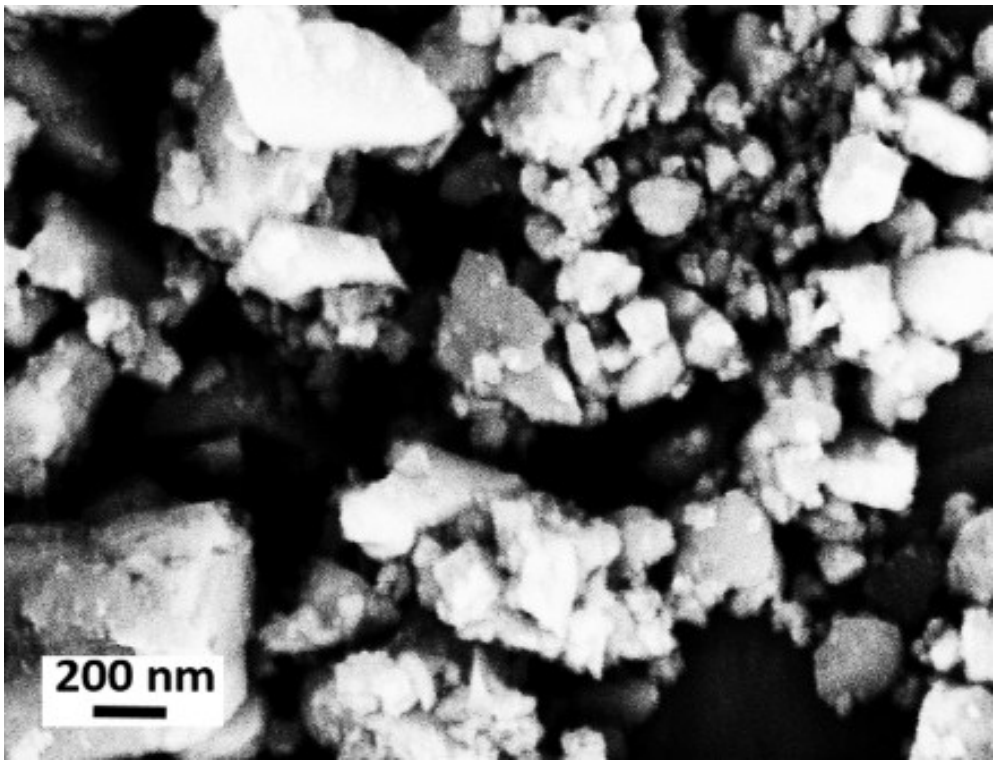

Fig. 2

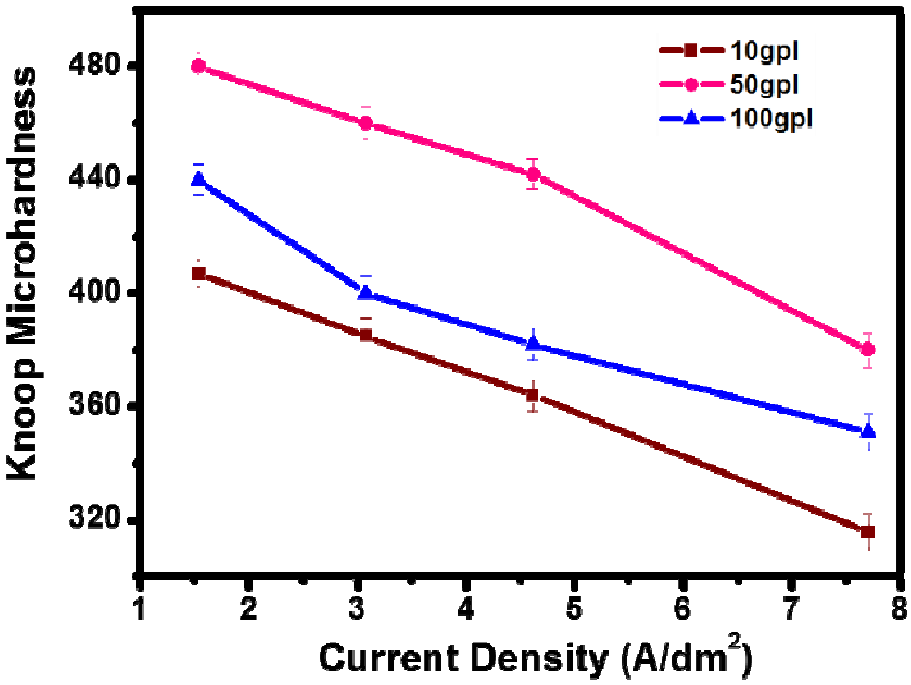

Fig.3

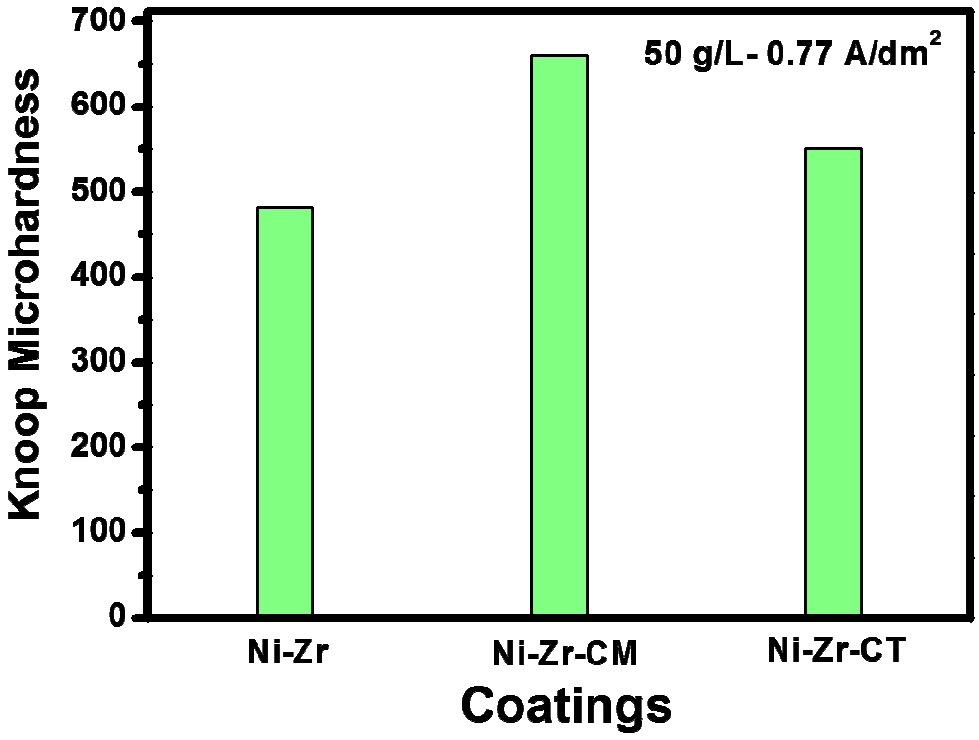

Fig.4

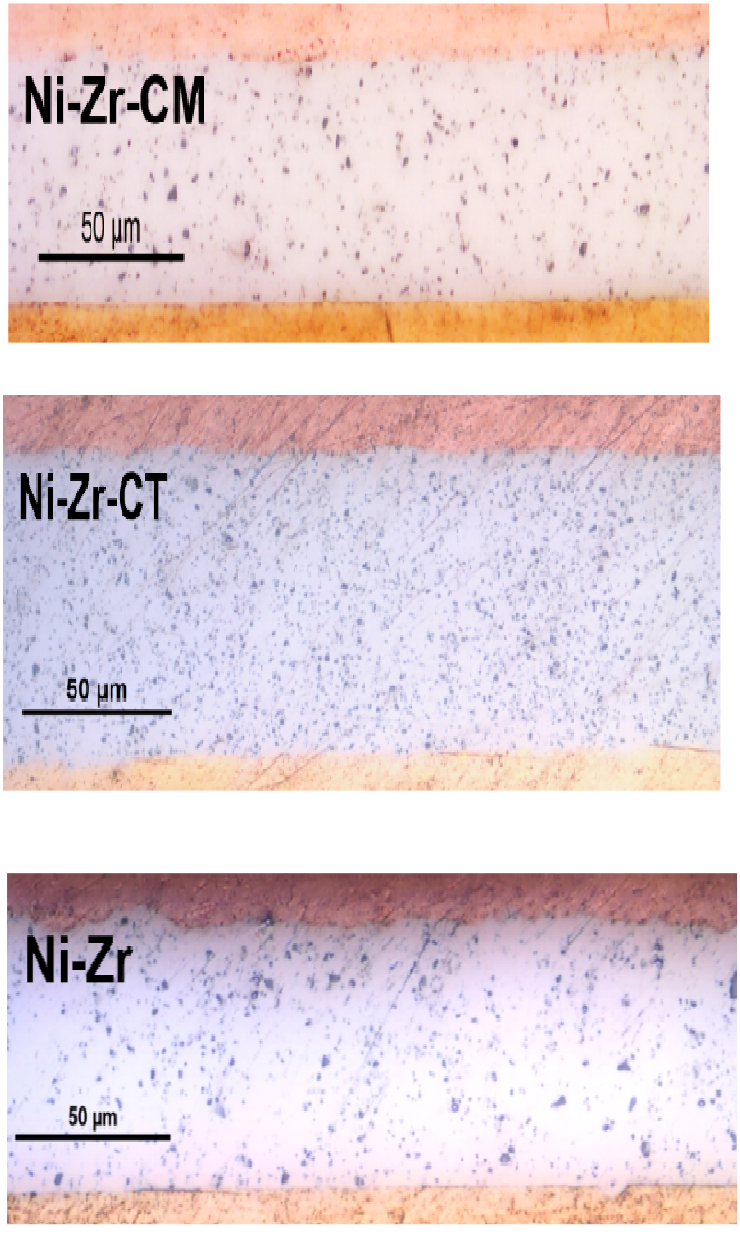

Fig.5

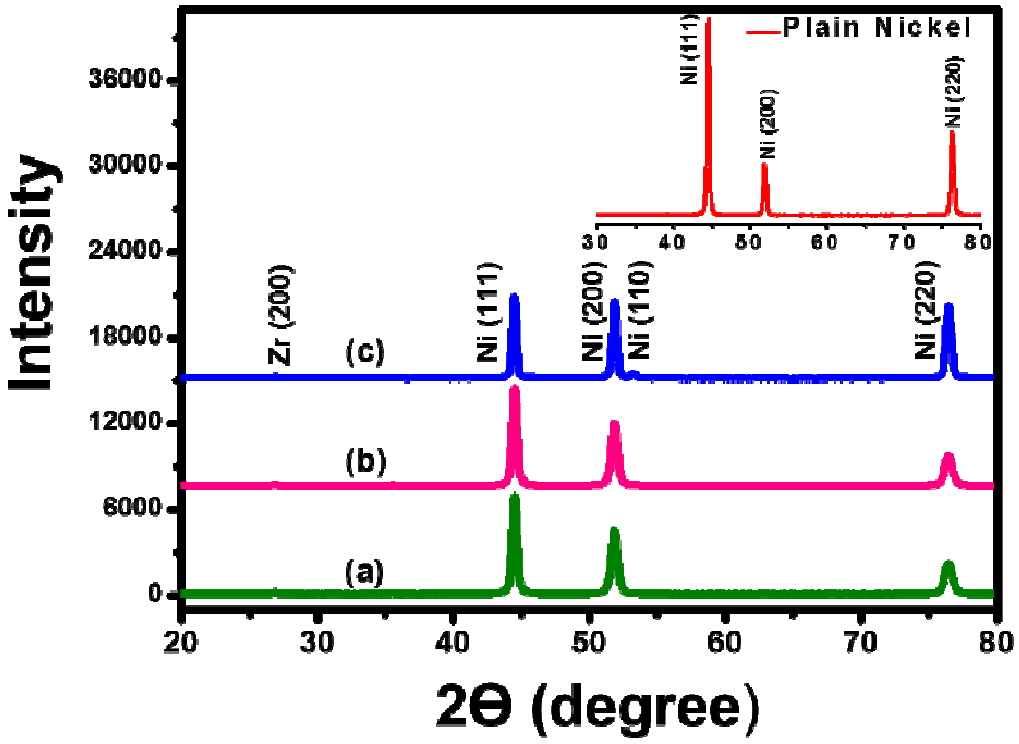

Fig.6

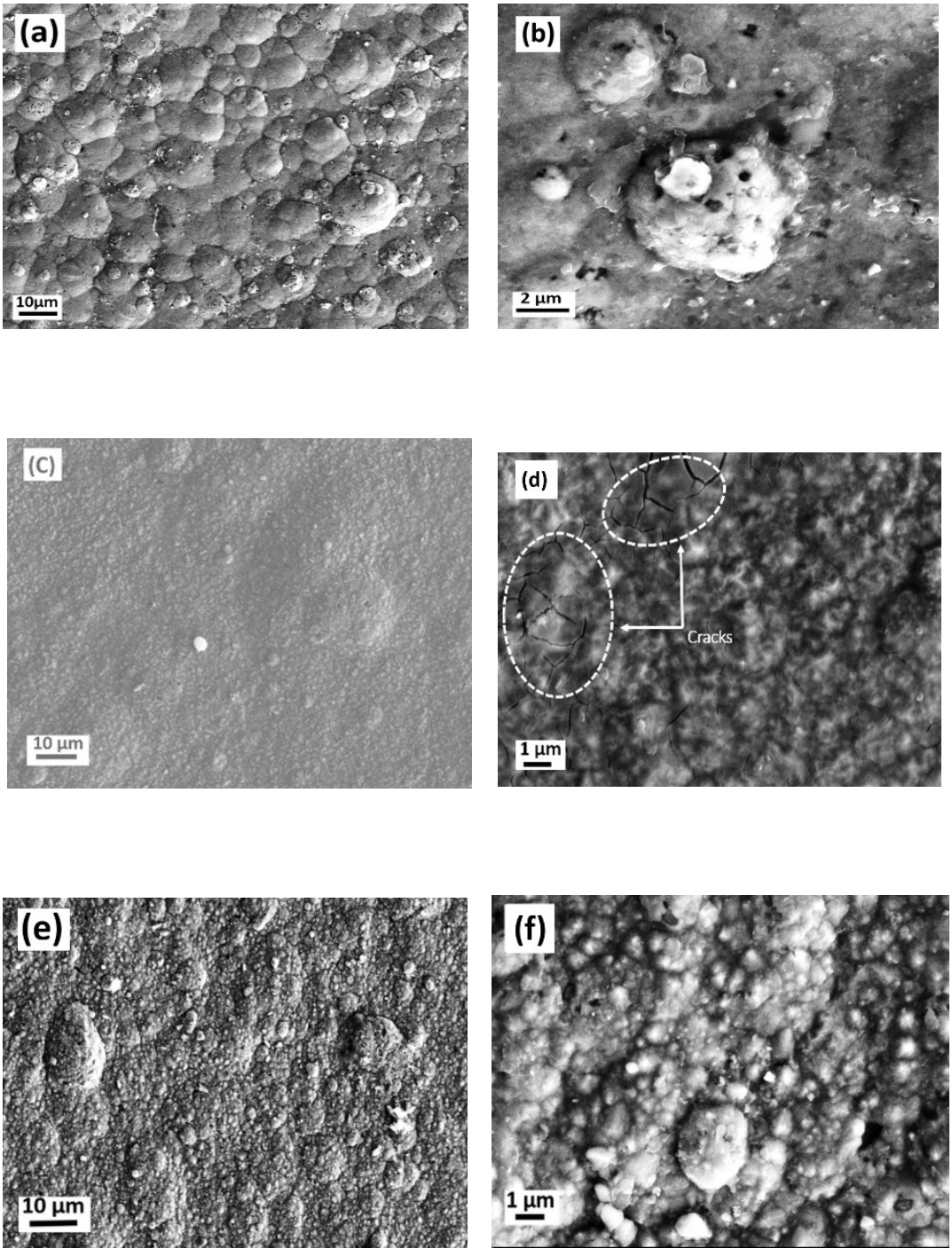

Fig.7

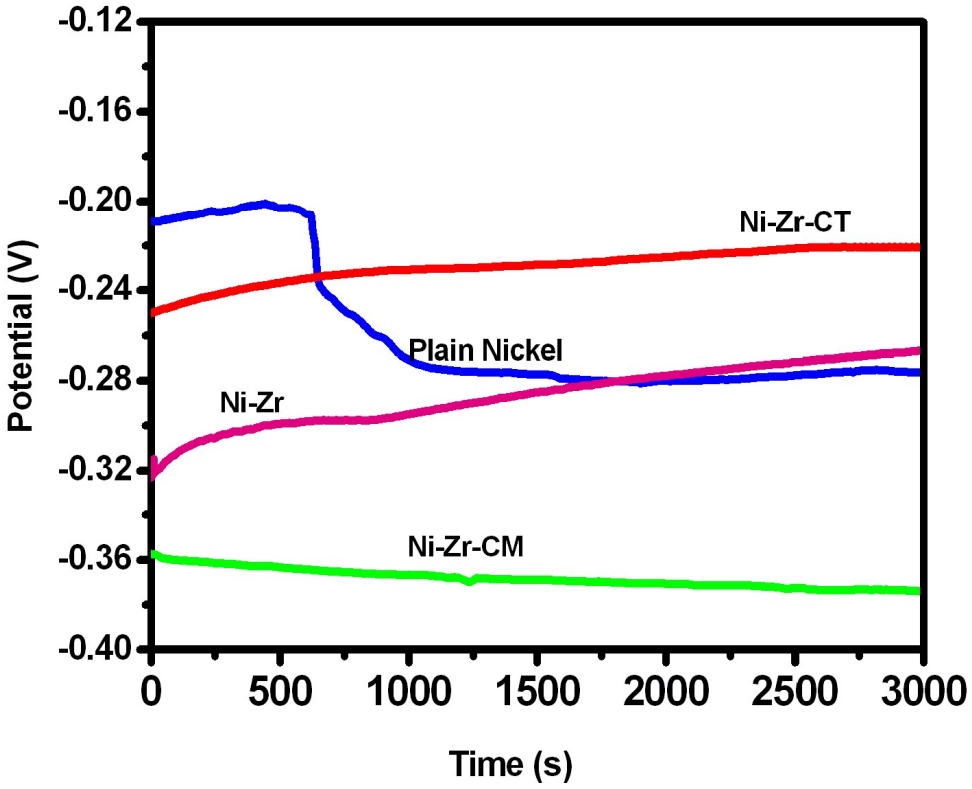

Fig.8.

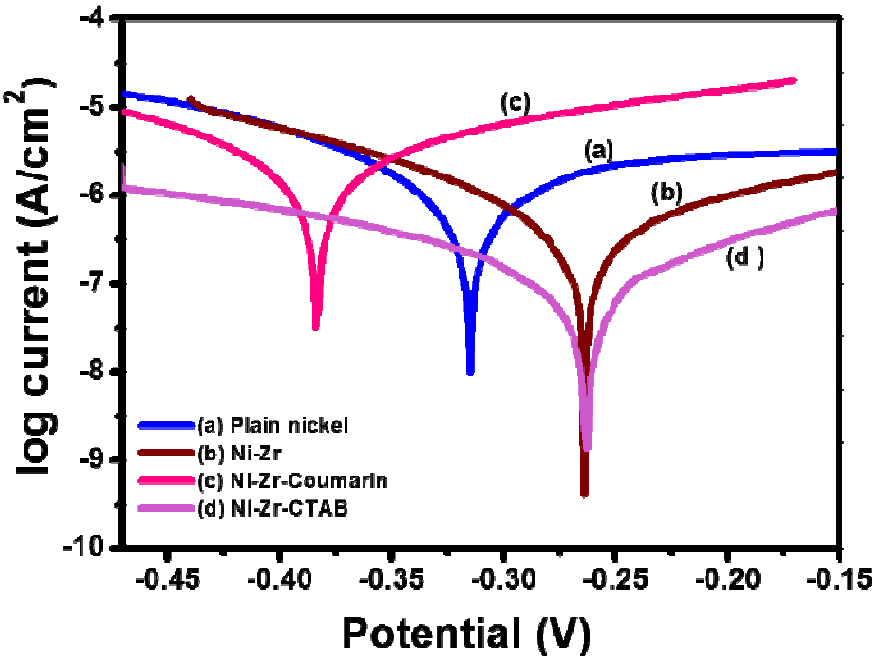

Fig.9

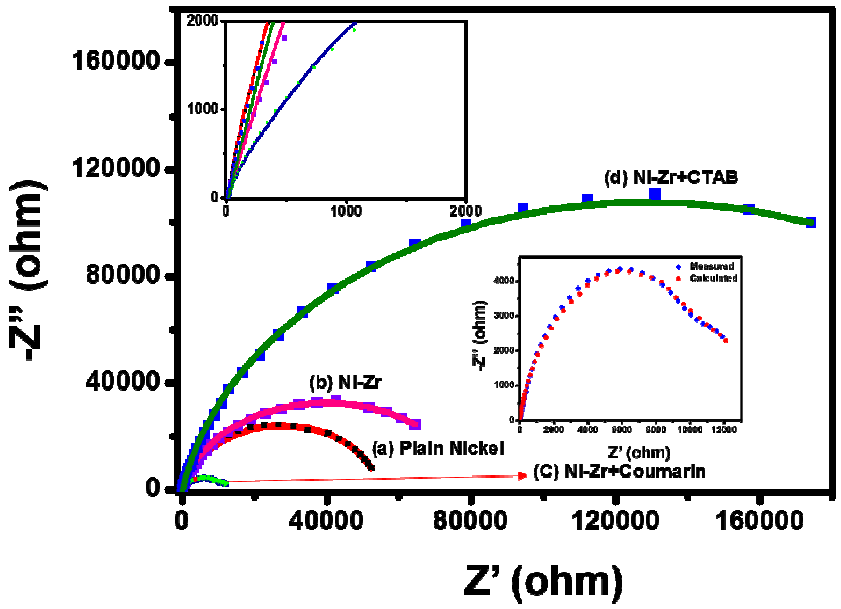

Fig.10

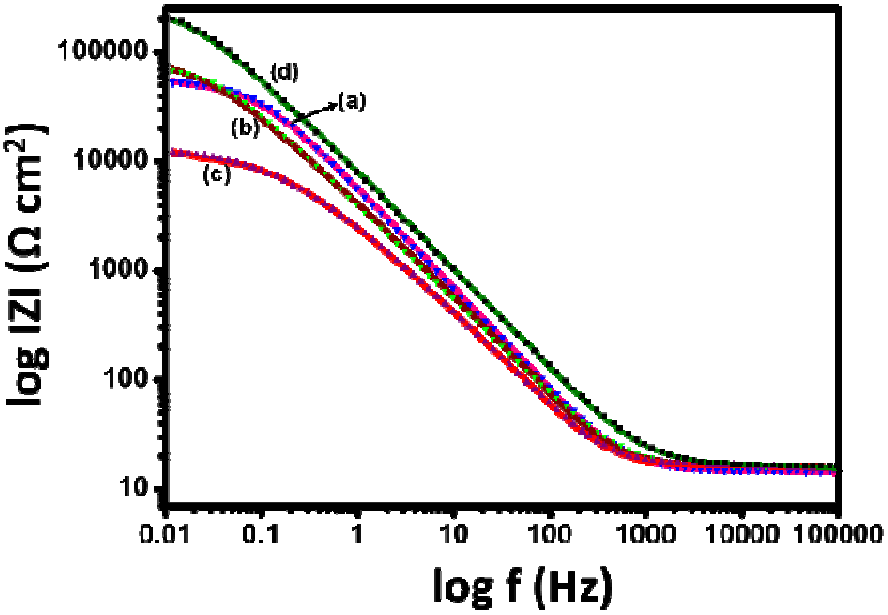

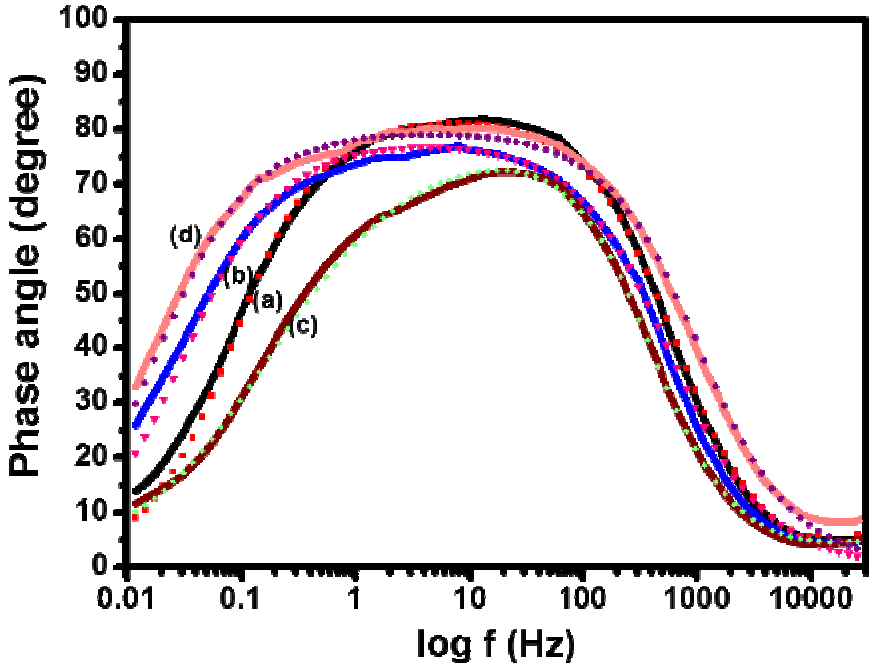

Fig.11

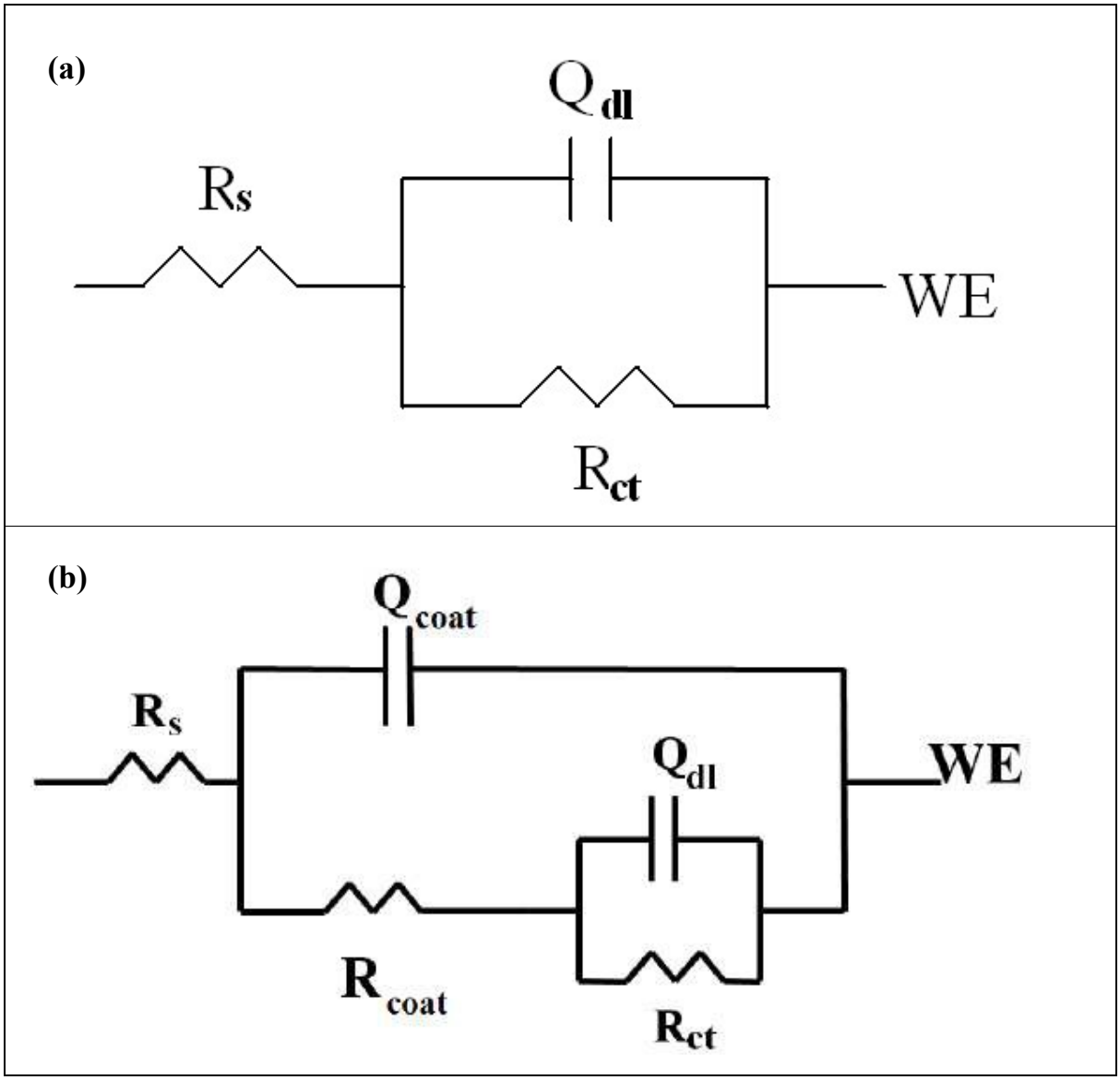

Fig.12